Cell. Mol. Life Sci. (2017) 74:2299–2318
DOI 10.1007/s00018-017-2461-9

Cellular and Molecular Life Sciences

ORIGINAL ARTICLE

# Membrane-traversing mechanism of thyroid hormone transport by monocarboxylate transporter 8

**Jonas Protze[1] · Doreen Braun[2] · Katrin Manuela Hinz[1] · Dorothea Bayer-Kusch[2] · Ulrich Schweizer[2] · Gerd Krause[1]**

Received: 16 August 2016 / Revised: 14 December 2016 / Accepted: 9 January 2017 / Published online: 28 January 2017


**Abstract** Monocarboxylate transporter 8 (MCT8) mediates thyroid hormone (TH) transport across the plasma membrane in many cell types. In order to better understand its mechanism, we have generated three new MCT8 homology models based on sugar transporters XylE in the intracellular opened (PDB ID: 4aj4) and the extracellular partly occluded (PDB ID: 4gby) conformations as well as FucP (PDB ID: 3o7q) and GLUT3 (PDB ID: 4zwc) in the fully extracellular opened conformation. $T_3$-docking studies from both sides revealed interactions with His192, His415, Arg445 and Asp498 as previously identified. Selected mutations revealed further transport-sensitive positions mainly at the discontinuous transmembrane helices TMH7 and 10. Lys418 is potentially involved in neutralising the charge of the TH substrate because it can be replaced by charged, but not by uncharged, amino acids. The side chain of Thr503 was hypothesised to stabilise a helix break at TMH10 that undergoes a prominent local shift during the transport cycle. A T503V mutation accordingly affected transport. The aromatic Tyr419, the polar Ser313 and Ser314 as well as the charged Glu422 and Glu423 lining the transport channel have been studied. Based on related sugar transporters, we suggest an alternating access mechanism for MCT8 involving a series of amino acid positions previously and newly identified as critical for transport.

**Keywords** MFS-transporter · Thyroid hormones · Membrane proteins · Structure–function study · Mutagenesis · Molecular modelling

**Abbreviations**

| | |
|---|---|
| AHDS | Allan–Herndon–Dudley syndrome |
| FucP | *E. coli* fucose/$H^+$ symporter |
| GlpT | Glycerol-3-phosphate transporter |
| GLUT3 | Glucose transporter 3 |
| $T_3$ | 3,3′,5-Triiodothyronie |
| $T_4$ | 3,3′,5,5′-Tetraiodothyronine |
| TH | Thyroid hormone |
| TM | Transmembrane |
| TMH | Transmembrane helix |
| XylE | *E. coli* D-xylose:$H^+$ symporter |

## Introduction

Thyroid hormones (TH) are amino acid derivatives carrying positive and negative charges. In order to reach their nuclear $T_3$-receptor, TH need transporter proteins to help them cross the plasma membrane. Several classes of transporter proteins with 12 transmembrane helices (TMH) are capable of TH transport including the organic anion transporters 2, 3 and 14 (Oatp2 and Oatp3, Oatp14) [1–3], monocarboxylate transporters 8 and 10 (MCT8 and MCT10) [4, 5] and also amino acid/

J. Protze and D. Braun, as well as U. Schweizer and G. Krause contributed equally to this work.

**Electronic supplementary material** The online version of this article (doi:10.1007/s00018-017-2461-9) contains supplementary material, which is available to authorized users.

✉ Ulrich Schweizer
uschweiz@uni-bonn.de

✉ Gerd Krause
gkrause@fmp-berlin.de

[1] Leibniz-Institut für Molekulare Pharmakologie (FMP), Robert-Rössle-Str. 10, 13125 Berlin, Germany

[2] Institut für Biochemie und Molekularbiologie, Rheinische Friedrich-Wilhelms-Universität, 53115 Bonn, Germany

polyamine/organocation (APC) type transporters like the L-type amino acid transporters 1 and 2 (Lat1, Lat2) [6–8], reviewed in [9]. Among these transporters, only MCT8 is specific for TH. The major function of MCT8 is the cellular import and export of 3,3′,5,5′-tetraiodothyronine ($T_4$, thyroxine as prohormone) and the active, nuclear TH-receptor-binding 3,3′,5-triiodothyronine ($T_3$) along their concentration gradients across the plasma membrane [5]. Mutations in MCT8/SLC16A2 lead to severe psychomotor retardation and TH abnormalities [10, 11], the so-called Allan–Herndon–Dudley syndrome (AHDS) [12]. Surprisingly, mice deficient in *Mct8* replicate the endocrinological phenotype of AHDS patients but do not show severe neurological impairment [13–15]. It is hypothesised that mice express compensating transporters during their embryonic development which are absent in humans. Indeed using a double knockout strategy, Mayerl et al. [16] showed that *Oatp1c1* is important for $T_4$ transport at the blood–brain-barrier (BBB) and demonstrated that *Mct8/Slco1c1* double knockout mice develop a neurological phenotype that impacts on brain development. Humans only show a weak OATP1C1 expression at the BBB [17] which might be one reason for the differences between mice and humans concerning thyroid hormone transport into brain.

Transmembrane transport is a dynamic process during which the transporter protein undergoes a series of conformational changes that allow the substrate to enter a cavity in the transporter from one side of the membrane and leave the cavity towards the other side. The fundamental folding pattern of 12 TMH major facilitator superfamily (MFS) transporters is characterised by two 6 TMH-bundles, an N-terminal bundle linked by an extended linker peptide to a C-terminal bundle [18]. Both 6 TMH-domains are composed of two 3 TMH-motifs which are symmetrical. The relative movement of the two 6 TMH-bundles is thought to allow the passage of substrate between the interfaces of both domains [18]. To fully appreciate the roles of specific amino acids in substrate recognition and conformational changes, transporter models in several conformations along the transport cycle are desirable.

There is still a lack of experimental structure information that explains substrate specificity for all TH transmembrane transporters. With the help of an initial molecular homology model of MCT8, based on the crystal structure of the bacterial glycerol-3-phosphate transporter GlpT in the intracellular facing conformation (PDB ID: 1pw4 [19]), we previously identified the highly conserved amino acids Arg445 (TMH8) and Asp498 (TMH10) of MCT8 as being involved in $T_3$-transport and verified their essential role experimentally by alanine mutations [20]. Our initial model also suggested that both residues are likely interacting. This was confirmed by further experiments showing that a reciprocal charge swap (R445D, D498R) rescued in part the severely reduced $T_4$ uptake of single mutants [21].

The ligand binding site in both TH-receptors (TRα and TRβ) was shown to consist of one histidine and two arginines [22, 23]. These residues bind $T_3$ between a "His–Arg clamp" as shown in the crystal structure of the $T_3$-receptor/$T_3$ complex (PDB ID: 3gws [23]). This prompted us to investigate whether such a motif might potentially be relevant for $T_3$ recognition in MCT8. Indeed, three potential "His–Arg clamps" were discovered in the MCT8 model formed by residue pairs His192/Arg301, His192/Arg445 and His415/Arg301, which matched the geometry of the $T_3$-receptor/$T_3$-pair [24, 25]. Previous [20] and recent experimental studies [21, 24, 26] confirmed the involvement of these residues in $T_3$-transport.

Moreover, reaction with Cys-specific chemical probes identified two out of ten cysteine residues (Cys481 and Cys497) as functionally important in MCT8 [27].

Our previous molecular model of MCT8 could not explain the molecular traversing mechanism of TH, since it illustrated only the intracellular accessible conformation, based on the intracellular opened crystal structure of the GlpT transporter. Recent progress in crystallography of related sugar transporters in three conformations has allowed us, for the first time, to generate models of MCT8 in several conformations along the transport cycle to better understand protein–substrate interactions. These models (extracellular opened, extracellular partly occluded and intracellular opened conformations) were probed by site-directed mutagenesis and transport was measured in cell models.

## Methods

### Modelling of MCT8

The MCT8 models in intracellular opened and extracellular partly occluded conformation were built on the crystal structures of xylose transporter XylE in intracellular opened (PDB ID: 4aj4 [28]) and extracellular partly occluded (PDB ID: 4gby [29]) conformation. Irregularities in the helices TMH5 and TMH7 (see sequence alignment in ESM_1) were corrected manually. Fragments used for manual adjustments in TMH5: π-helix fragment from PDB ID: 2qd3 [30] residues 351–355 and in TMH7: fragment from GlpT, PDB ID: 1pw4 [19] residues 265–269. Loops were created utilising the Loop Search tool implemented in Sybyl X2.1.1 (Certara USA Inc., St. Louis, MO, USA). The structure of glucose transporter GLUT3 in the extracellular opened conformation (PDB ID: 4zwc [31]), as well as the structure of fucose transporter FucP in the extracellular opened conformation (PDB ID: 3o7q [32]) were utilised

as matrices to achieve a fully extracellular opened conformation of MCT8, by overlaying the N- and C-terminal domains (Helices 1–6 and 7–12) of the extracellular partly occluded model of MCT8 separately with the according domains of GLUT3 (4zwc) and FucP (3o7q) followed by manual reconcatenating. All manual dockings, manipulations, optimisations of the models, as well as calculations of hydrophobic and electrostatic potentials on the molecular surfaces, were performed with Sybyl X2.1.1 (Certara USA Inc., St. Louis, MO, USA). Models were energetically minimised using the AMBER7 FF99 force field. Structure images and morphs between intracellular opened, extracellular partly occluded and extracellular opened conformations were generated with PyMOL 1.8.0.1 [33].

### Site-directed mutagenesis, cell culture and TH-uptake assays

Mutations of N-terminal HA tagged wild-type MCT8 were introduced by site-directed mutagenesis (QuikChange Lightning Site-Directed Mutagenesis Kit, Stratagene) using the oligonucleotides shown in Table 1. All selected residues for substitutions are >90% conserved among 100 closest orthologous of MCT8 and also highly similar in human MCT10 (see Table in ESM_2).

Stable transfection of Madin Darby canine kidney (MDCK1) cells, kinetic experiments with radioactive labelled $^{125}$I-$T_3$ (Perkin Elmer), western blotting and surface biotinylation as well as injection of *Xenopus laevis* oocytes with cRNA were performed as described elsewhere [34–36]. All uptake experiments have been performed two to three times (in triplicates) with similar results and one representative experiment is shown unless otherwise indicated. Statistical calculations were done with GraphPad Prism 6. MDCK1 cells do not express endogenous thyroid hormone transporters and have little background uptake activity [37]. For that reason MDCK1 cells have been chosen as a model.

## Results

We searched for templates in the PDB among the major facilitator superfamily (MFS) transporters for which crystal structures exist in more than one state. As closest match in sequence similarity we found the crystal structures of the xylose transporter XylE (*E. coli*) in the intracellular opened (PDB ID: 4aj4 [28]) and the extracellular partly occluded (PDB ID: 4gby [29]) states. We also used the human glucose transporter GLUT3 in the extracellular partly occluded (PDB ID: 4zw9; 4zwb [31]) and extracellular opened (PDB ID: 4zwc [31]) states. We, therefore, created a revised MCT8 homology model in the intracellular opened conformation based on the respective XylE structure (PDB ID: 4aj4 [28]) which is very similar to our previous model based on GlpT [20]. The second MCT8 model based on the extracellular partly occluded crystal structure of XylE (PDB ID: 4gby [29]) is not fully opened to the extracellular side, which hinders an extracellular entry or release of THs. This applies also to the conformation of the extracellular partly occluded conformation (PDB ID: 4zw9; 4zwb [31]) of GLUT3 with bound D-glucose. Thus, the second new model represents an intermediate state of MCT8 in an extracellular partly occluded state with bound ligand.

The crystal structures of GLUT3 (PDB ID: 4zwc [31]) and of another sugar transporter, fucose transporter FucP (PDB ID: 3o7q [32]) are in a fully extracellular opened conformation and thus allow for extracellular entry or release of the respective substrate.

To understand the conformational transition in XylE from the intracellular opened (PDB ID: 4aj4, Fig. 1a, dark grey) to the extracellular partly occluded state (PDB ID: 4gby, Fig. 1a, yellow) we superimposed the Cα atoms of only the N-terminal domain (Tyr9–Glu222, TMH1–TMH6) of the two states and only the C-terminal domain (Val275–Ala455, TMH7–TMH12) of the two XylE states separately (Fig. 1a). Structural differences between the two N-terminal and the two C-terminal 6 TMH-domains in each conformational state resulted in an RMSD over Cα atoms of 0.67 Å for the N-terminal domain and of 0.94 Å for the C-terminal domain, respectively. This indicates that each 6 TMH-domain remains more or less rigid within the overall 6 TMH arrangement in both conformational states. The major conformational transition is thus a rigid body movement by tilting the N- and C-terminal domain relative to each other around a central ligand recognition cavity. This applies also for the corresponding N-terminal domains of GLUT3 in the extracellular partly occluded and in the fully extracellular opened (RMSD = 0.47 Å) states as well as for the C-terminal domain in the respective states (RMSD = 0.43 Å). However, for the C-terminal domain of GLUT3, where TMH7 and TMH10 are discontinuous helices (named TMH7a/7b and TMH10a/10b, respectively) a prominent local rearrangement is reported to occur for TMH7b at the extracellular side [31]. Notably, a glycine (invariant Gly284 in GLUT3 and also Gly292 in XylE) constitutes in both cases a bulge preceding TMH7b, which may provide the flexibility for the pronounced structural shift observed in GLUT3. However, this obvious inserted bulge forming glycine in GLUT3 and XylE is absent in the sequences of FucP, GlpT, MCT8 and MCT10 and, therefore, causes a gap in the corresponding sequence alignment (see sequence alignment in ESM_1). Subsequently the structures of FucP and GlpT show only a slight helix discontinuity and not such a pronounced bulge compared to XylE and GLUT3. Therefore, we used FucP (PDB ID:

**Table 1** Oligonucleotides used for site-directed mutagenesis of MCT8

| Primer | Sequence |
|---|---|
| E422D | |
| fwd | GATGAAGTATGTGGAGGACGAGTTCTCAGAAATCAAG |
| rev | CTTGATTTCTGAGAACTCGTCCTCCACATACTTCATC |
| E422N | |
| fwd | CCTGATGAAGTATGTGGAGAACGAGTTCTCAGAAATCAAGG |
| rev | CCTTGATTTCTGAGAACTCGTTCTCCACATACTTCATCAGG |
| E423D | |
| fwd | GAAGTATGTGGAGGAGGACTTCTCAGAAATCAAGGAG |
| rev | CTCCTTGATTTCTGAGAAGTCCTCCTCCACATACTTC |
| E423N | |
| fwd | TGATGAAGTATGTGGAGGAGAACTTCTCAGAAATCAAGGAGAC |
| rev | GTCTCCTTGATTTCTGAGAAGTTCTCCTCCACATACTTCATCA |
| K418R | |
| fwd | CTATGTACACCTGATGAGGTATGTGGAGGAGGAGT |
| rev | ACTCCTCCTCCACATACCTCATCAGGTGTACATAG |
| K418A | |
| fwd | CCCTATGTACACCTGATGGCGTATGTGGAGGAGGAGTTC |
| rev | GAACTCCTCCTCCACATACGCCATCAGGTGTACATAGGG |
| K418E | |
| fwd | CTATGTACACCTGATGGAGTATGTGGAGGAGGAGT |
| rev | ACTCCTCCTCCACATACTCCATCAGGTGTACATAG |
| K418Q | |
| fwd | CTATGTACACCTGATGCAGTATGTGGAGGAGGAGT |
| rev | ACTCCTCCTCCACATACTGCATCAGGTGTACATAG |
| R388Q | |
| fwd | TGCGTTGGCGGAACACTTGCATGTTGAAGTACTTC |
| rev | GAAGTACTTCAACATGCAAGTGTTCCGCCAACGCA |
| R388K | |
| fwd | AGTGCGTTGGCGGAACACTTTCATGTTGAAGTACTTCCTG |
| rev | CAGGAAGTACTTCAACATGAAAGTGTTCCGCCAACGCACT |
| R388E | |
| fwd | AGGAAGTACTTCAACATGGAAGTGTTCCGCCAACGCAC |
| rev | GTGCGTTGGCGGAACACTTCCATGTTGAAGTACTTCCT |
| R388M | |
| fwd | GTAAGTGCGTTGGCGGAACACCATCATGTTGAAGTACTTCCTGAG |
| rev | CTCAGGAAGTACTTCAACATGATGGTGTTCCGCCAACGCACTTAC |
| S313A | |
| fwd | GGTGTGGTGTCTGCTGGGGCTAGCATTTTCTCCATGTC |
| rev | GACATGGAGAAAATGCTAGCCCCAGCAGACACCACACC |
| S314A | |
| fwd | GTGGTGTCTGCTGGGAGTGCCATTTTCTCCATGTCCTT |
| rev | AAGGACATGGAGAAAATGGCACTCCCAGCAGACACCAC |
| T503V | |
| fwd | GCGATGGCTTCTTCATCGTCATCATGGCCCCCATTG |
| rev | CAATGGGGGCCATGATGACGATGAAGAAGCCATCGC |
| Y419V | |
| fwd | CTATGTACACCTGATGAAGGTTGTGGAGGAGGAGTTCTCA |
| rev | TGAGAACTCCTCCTCCACAACCTTCATCAGGTGTACATAG |
| Y419W | |
| fwd | TATGTACACCTGATGAAGTGGGTGGAGGAGGAGTTCTCAG |
| rev | CTGAGAACTCCTCCTCCACCCACTTCATCAGGTGTACATA |

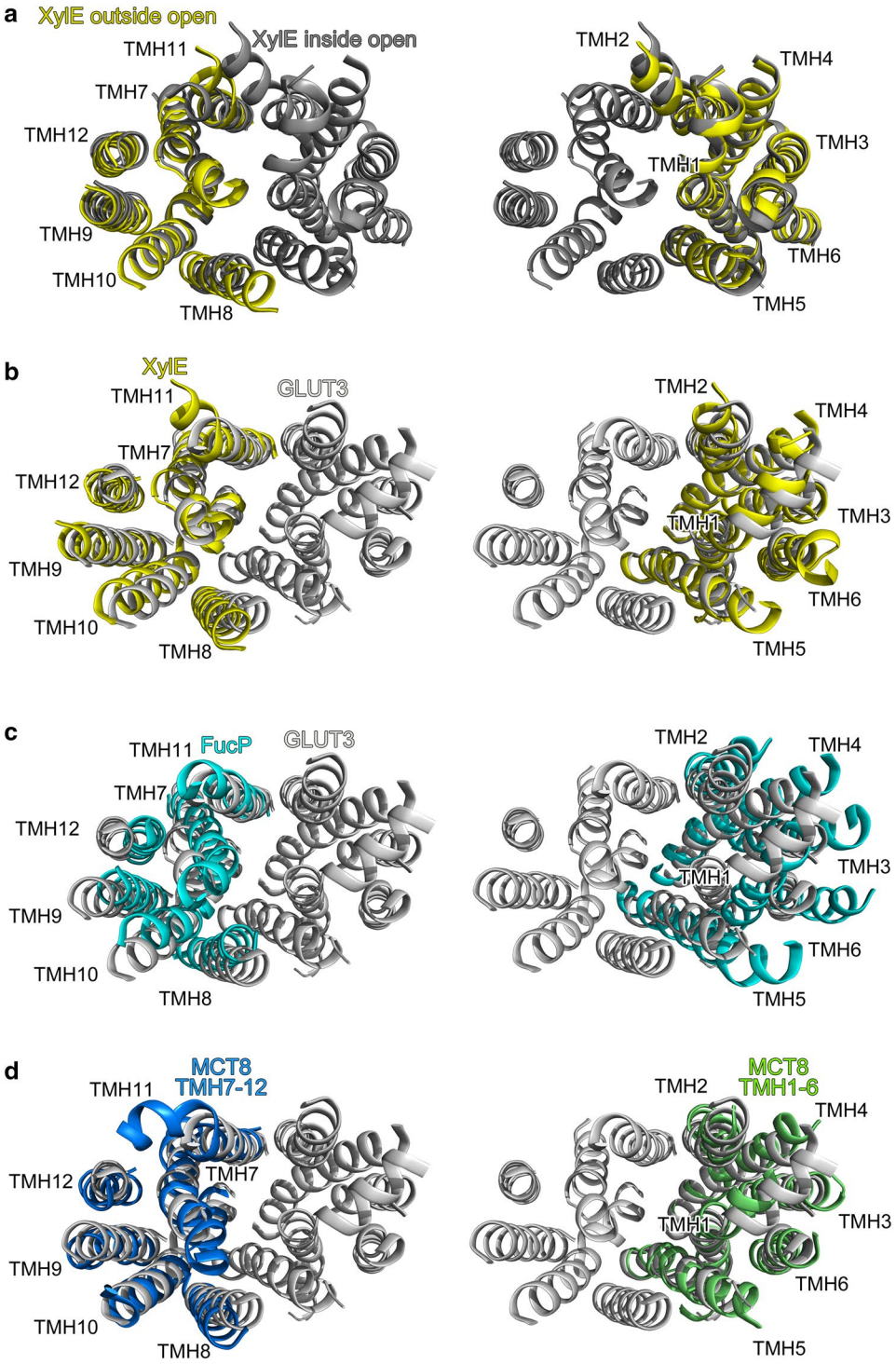


**Fig. 1** Separate overlay of the N-terminal (*right panels*) and C-terminal (*left panels*) 6 TMH-bundle domains of **a** intracellular opened (PDB ID: 4aj4, *dark grey*) and extracellular partly occluded (PDB ID: 4gby, *yellow*) crystal structures of XylE; **b** fully extracellular opened crystal structure of GLUT3 (PDB ID: 4zwc, *light grey*) and extracellular partly occluded structures of XylE (PDB ID: 4gby, *yellow*); **c** fully extracellular opened crystal structure of GLUT3 (PDB ID: 4zwc, *light grey*) and fully extracellular opened crystal structures of FucP (PDB ID: 3o7q, *cyan*); **d** the MCT8 model based on PDB ID: 4gby (TMH1-6: *green*; TMH7-12: *blue*) and fully extracellular opened crystal structure of GLUT3 (PDB ID: 4zwc, *light grey*) reveal high similarity in the arrangement of the 6 TMH-bundles. This result allowed the generation of a full extracellular opened MCT8 model by tilting one of the 6 TMH-bundles according the pivot of the channel interface

3o7q [32]) as structural template for these TMH7-positions in our MCT8 models.

In TMH10 a N-terminal helix capping Gly-Pro motif that follows a helix break is conserved in the sequence of TMH10b as in many transporters such as GLUT3, XylE, GlpT and also in FucP (as Tyr-Pro) (see sequence alignment in ESM_1). In our alignment, residue Thr503 of TMH10 is placed at the corresponding position of the TMH10b-capping motif. Thus it is very likely that the helix capping is stabilised by a Thr side chain interaction with the backbone carboxyl group and that a similar interruption of TMH10 occurs also in MCT8. We used XylE as template for TMH10 in MCT8.

These facts were integrated to achieve a fully extracellular opened model of MCT8. We superimposed the two extracellular partly occluded structures of XylE and GLUT3. The corresponding fully extracellular opened crystal structure of GLUT3 (PDB ID: 4zwc [31]) was used as a structural matrix. The 6 TMH-bundles of the N- and C-terminal domains of extracellular partly occluded XylE (Fig. 1b, yellow) show a striking similarity in the arrangement to the corresponding domains of the fully extracellular opened conformation of GLUT3 (Fig. 1b, light grey), when separately overlaid. Pairwise fitting of Cα atoms of the respective XylE and GLUT3 domains revealed an RMSD of 1.20 Å for the N-terminal and an RMSD of 1.10 Å for the C-terminal domain. Thus, the separate 6 TMH-bundle subunits of the extracellular partly occluded MCT8 model based on XylE (PDB ID: 4gby), were structurally aligned to the corresponding subunits of GLUT3 (PDB ID: 4zwc) with particular focus on the channel interface by computer-assisted reciprocal tilting of the 6 TMH-bundles accordingly (Fig. 1b, yellow helices).

The crystal structure of a fully extracellular opened state from FucP was used for comparison. The extracellular opening angle between the 6 TMH-bundles of the N- and C-terminal domains for the extracellular opened conformations from GLUT3 and FucP showed a striking similarity (Fig. 1c).

This resulted in a new third MCT8 model of the fully extracellular opened conformation (based on PDB ID: 4gby and PDB ID: 4zwc, Fig. 2a, b) which is useful for $T_3$-docking.

## Extra- and intracellular T3-docking reveals one central substrate recognition and membrane-traversing cavity

The MCT8 models in the extra- and intracellular open conformations were used for $T_3$-docking studies. One central substrate recognition cavity was apparent, which is formed and shaped by the previously described transport-sensitive residues His192, His415 [24, 26] and Arg445, Asp498 [20, 21] as well as Cys497 [27]. Our new models based on homologous MFS transmembrane transporters revealed that these residues are accessible both from the extracellular side and from the intracellular side in conformations open towards these compartments (Fig. 2d, e). Moreover, the three different MCT8 models (extracellular opened, extracellular partly occluded and intracellular opened) suggest the following potential molecular transport mechanism. After extracellular recognition, $T_3$ adheres alternately to these residues in the central recognition and traversing cavity. The banana-shaped N- and C-terminal domains are tilting around the central TH recognition site (Fig. 2f–h) with alternating extra- and intracellular accessibility of the known transport-sensitive MCT8 residues (Fig. 2d, e). In doing so, the $T_3$ binding sites likely undergo a dynamic rearrangement during the transport cycle (see morph between the three conformational MCT8 models in ESM_3) in which $T_3$ is lifted through the central traversing channel and released towards the intracellular side and vice versa.

In addition to the previously postulated His–Arg clamps for THs between His415–Arg301, His192–Arg301 and His192–Arg445 [24, 25] the new models allow for a fourth His–Arg clamp between His415–Arg445. The His–Arg clamp pairs His415–Arg445 and His192–Arg445 both are accessible for $T_3$ in the extracellular as well as in the intracellular opened conformation of the MCT8 model, whereas the His–Arg clamps formed by His192, His415 and Arg301 are only accessible in the intracellular opened conformation. In that context it is to be noted that DEPC as a His-reactive probe applied in the medium only modified His192, but not His415 [26].

The differing His–Arg clamps may be engaged consecutively during a transport cycle. The charge interaction between Arg445–Asp498 can be observed in all three new MCT8 conformations as suggested in our previous model [20] and confirmed experimentally by Groeneweg et al. 2014 [21]. Even the previously postulated interaction of Arg445 and Asp498 with $T_3$ [20] is replicated in all three states. Cys497 is pointing into the traversing cavity in all three models. This is in agreement with its experimental accessibility by *p*-chloromercurybenzenesulfonate (pCMBS) that blocks $T_3$-uptake by obstructing the traversing cavity. The mutation C497A rescues $T_3$-uptake in the presence of pCMBS [27]. The three new models thus are compatible with biochemical findings obtained by different groups using different approaches, lending further support to the new models of MCT8.

## The role of Lys418, a charged amino acid in the membrane plane close to the substrate cavity

The lifting processes of $T_3$ through the central traversing cavity suggested by the new MCT8 models identified Lys418 as a further residue that likely takes part as interaction partner in the alternating $T_3$ interactions. Lys418 is located in TMH7 at the surface facing the transport channel. Moreover, it is situated at the presumed bulge region of TMH7 and may thus be critical for conformational changes of the transporter. Model guided mutagenesis of Lys418 (Fig. 3) revealed that mutation K418A abolished $T_3$-uptake activity. This effect is stronger than could be explained by its weaker expression in MDCK1 cells and *Xenopus* oocytes. We hypothesised that a charge at this position may be critical for function and introduced Arg and Glu at this position. Mutation K418R even increased $T_3$-uptake activity. Quite surprisingly, the charge

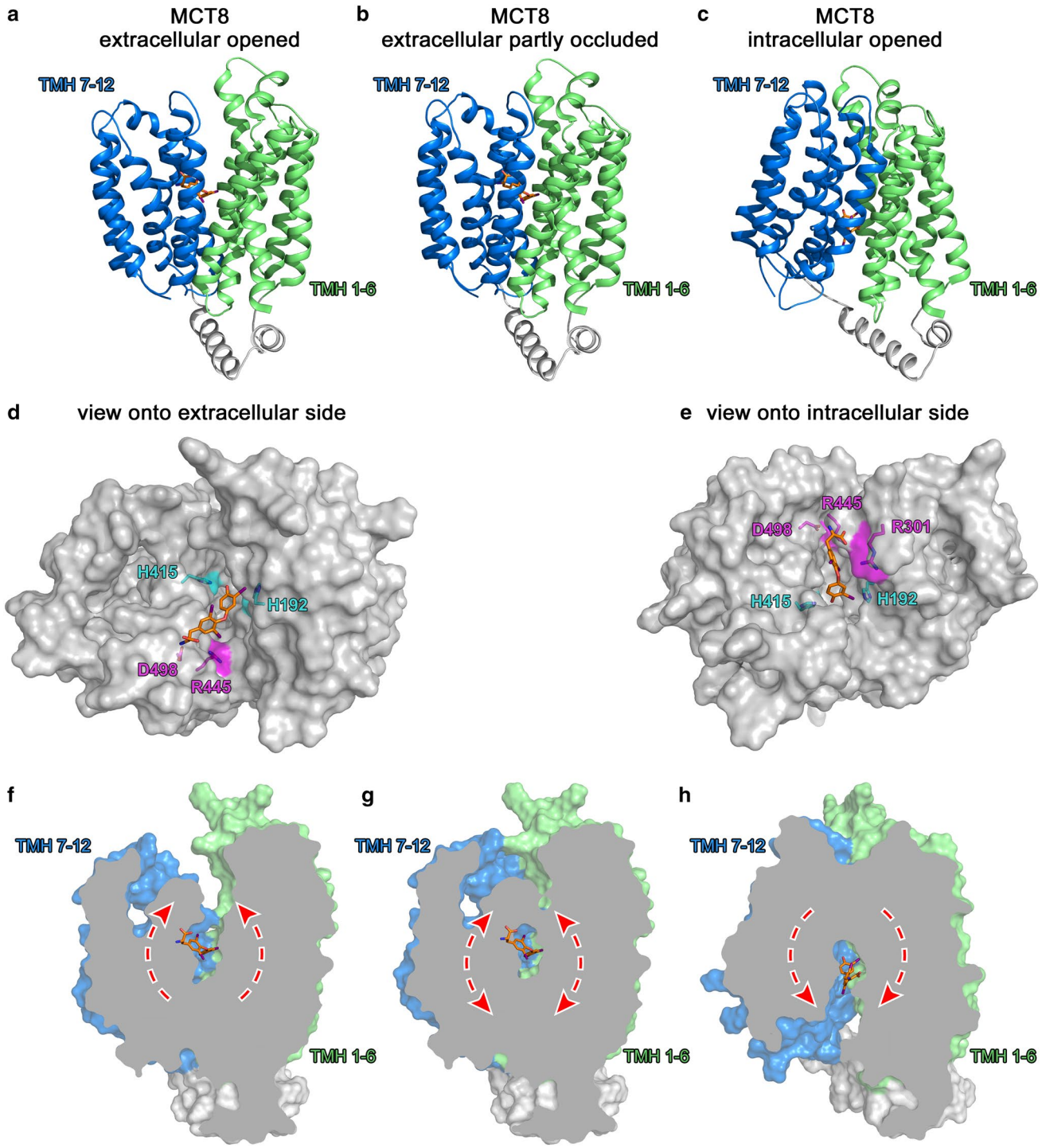


**Fig. 2** **a, d, f** MCT8 models of extracellular opened, **b, g** extracellular partly occluded and **c, e, h** intracellular opened conformations (based on crystal structures of XylE, GLUT3 and FucP) reveal one central substrate recognition and membrane-traversing cavity. **d, e** The central cavity is formed by previously reported transport-sensitive residues such as His415, His192 (*cyan*), Arg445 and Asp498 (*magenta*) which are accessible from both sides. Arg301 (*magenta* in **e**) is only accessible from the intracellular side. **f–h** After extracellular recognition $T_3$ adheres to these residues during tilting (*red arrows*) of the N- (*green*) and C-terminal (*blue*) 6 TMH-bundles around the central cavity and is thus lifted through the central traversing channel and released towards the intracellular side and vice versa

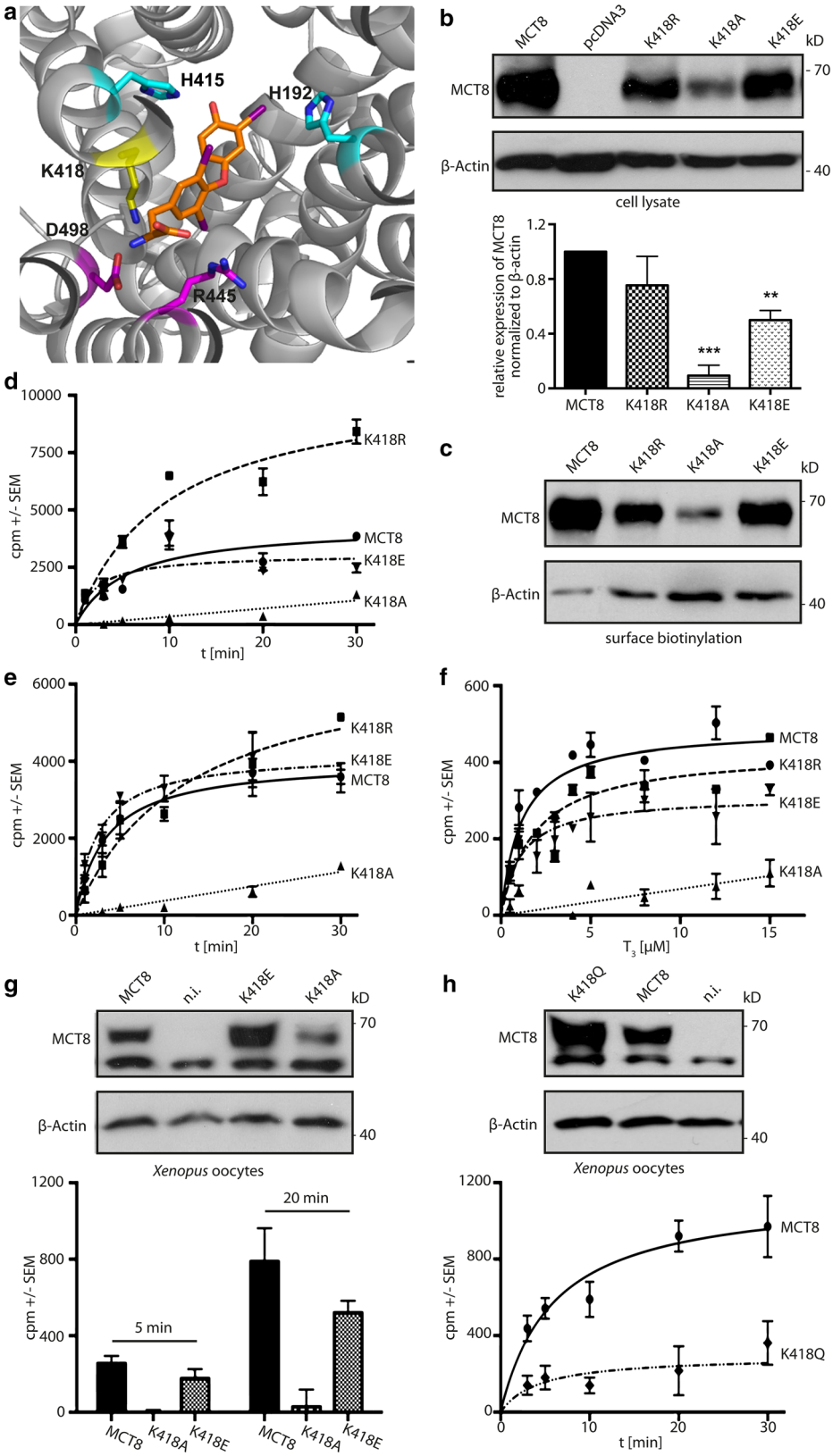
a
H415
H192
K418
D498
R445
b
MCT8
pcDNA3
K418R
K418A
K418E
kD
MCT8
β-Actin
70
40
cell lysate
relative expression of MCT8 normalized to β-actin
1.2
0.8
0.4
0
***
**
MCT8
K418R
K418A
K418E
c
MCT8
K418R
K418A
K418E
kD
MCT8
β-Actin
70
40
surface biotinylation
d
cpm +/- SEM
10000
7500
5000
2500
0
K418R
MCT8
K418E
K418A
0
10
20
30
t [min]
e
cpm +/- SEM
6000
4000
2000
0
K418R
K418E
MCT8
K418A
0
10
20
30
t [min]
f
cpm +/- SEM
600
400
200
0
MCT8
K418R
K418E
K418A
0
5
10
15
T3 [μM]
g
MCT8
n.i.
K418E
K418A
kD
MCT8
β-Actin
70
40
Xenopus oocytes
cpm +/- SEM
1200
800
400
0
20 min
5 min
MCT8
K418A
K418E
MCT8
K418A
K418E
h
K418Q
MCT8
n.i.
kD
MCT8
β-Actin
70
40
Xenopus oocytes
cpm +/- SEM
1200
800
400
0
MCT8
K418Q
0
10
20
30
t [min]

◂**Fig. 3** A charge (irrespectively whether positive or negative) is needed at position 418 for transport of $T_3$. **a** Partial view of MCT8 model. Lys418 (*sticks, yellow*) points into the central traversing cavity of MCT8 (*cartoon, grey*) formed by Arg445, Asp498 (*sticks, magenta*), His192 and His415 (*sticks, cyan*). The substrate $T_3$ is shown in *orange* as *sticks*. **b** Expression levels of different Lys418 mutants compared to wild-type MCT8. Western blot of 50 µg whole cell homogenates against MCT8. MDCK1 cells transfected with pcDNA3 empty vector served as negative control. β-Actin was used as a loading control. Quantification of western blots was performed on three replicates by densitometry. One-way ANOVA, Dunnett's test with $^{**}p<0.01$ and $^{***}p<0.001$. **c** Surface biotinylation of Lys418 mutants compared to $MCT8^{WT}$. **d** Time course uptake with 10 nM $^{125}$I-$T_3$ of $MCT8^{WT}$, K418R, K418A and K418E. The background of empty-vector transfected cells (pcDNA3) was subtracted from saturation curves. **e** Efflux of radioactive labelled $T_3$ by different Lys418 mutants was measured in the media over time after loading the cells with 10 nM $^{125}$I-$T_3$ for 45 min. **f** Determination of $K_M$ values for K418R, K418E and K418A compared to $MCT8^{WT}$ in stably transfected MDCK1 cells. $T_3$ concentration ranges from 0.5 to 15 µM. The uptake of different concentrations of $T_3$ was measured for 3 min. Empty-vector transfected cells served as background control and values were subtracted from saturation curves. $K_M$ (MCT8) = 2.7 ± 0.6 µM; $K_M$ (K418R) = 4.0 ± 1.0 µM; $K_M$ (K418E) = 4.3 ± 1.2 µM. **g** Injection of *Xenopus* oocytes with 30 ng capped cRNA of wild-type MCT8, K418A and K418E confirmed the results found in stably transfected MDCK1 cells. *Upper panel* western blot against MCT8 and β-actin (loading control). Non-injected oocytes served as negative controls. An unspecific band was found slightly smaller than MCT8. *Lower panel* end point assay with 10 nM $^{125}$I-$T_3$. The background of non-injected oocytes was subtracted. **h** *Xenopus* oocytes injected with K418Q. *Upper panel* western blot against MCT8. β-Actin served as a loading control. *Lower panel* time course uptake of K418Q compared to wild-type MCT8 with 10 nM $^{125}$I-$T_3$. Background of non-injected cells was subtracted from saturation curves

changing mutation K418E did not substantially alter uptake activity. These findings are supported by kinetic studies revealing $K_M$ values of $MCT8^{WT}$ = 2.7 ± 0.6 µM; K418R = 4.0 ± 1.0 µM and K418E = 4.3 ± 1.2 µM. These data indicate that the presence of a charge at position 418 is more critical than its sign. To further probe this idea, we replaced lysine with the isosteric, but uncharged, glutamine. However, we repeatedly failed to recover stable MDCK1 clones expressing K418Q. Therefore, *Xenopus* oocytes were injected with respective cRNA and despite significant expression, the activity of the mutant protein was very low, not allowing reasonable determination of a Michaelis constant. These findings suggest to us that the charge at position 418 may interact with the zwitterionic substrate to compensate the charges during passage through the hydrophobic membrane/protein environment. The K418A mutation, in contrast, may simply create a hole in the structure. Since the expression of K418A is diminished in two cell models, MDCK1 cells as well as *Xenopus* oocytes, a charge at position 418 is probably not only important for transport function but also affects protein folding or stability.

## Tyr419 may close the traversing cavity, but does not interact specifically with the substrate

In the MCT8-model Tyr419 is located one helix turn above H415 towards the extracellular side (Fig. 4) and could thus be involved in closing of the traversing cavity and also interact with the substrate. Mutation to Val reduces $T_3$-uptake and efflux, which is most likely related to decreased expression. In order to test if an aromatic moiety is needed for a stable expression, we created the substitution Tyr419 to tryptophan. This mutation only mildly affected expression and transport (slight increase of $K_M$), suggesting that an aromatic residue is needed at this position probably rather for protein stability than transport function. This is in agreement with the model where Tyr419 is interacting with the sulphur of Met225 in the intracellular opened state, stabilising this conformation like a latch.

## Polar Ser313 and Ser314 are essential for MCT8 stability and surface translocation

We investigated whether two consecutive serine residues which are located in a helix irregularity (bulge in TMH5) and line the central substrate channel (Fig. 5) are involved in substrate transport with their hydroxyl groups. Ser313 and Ser314 were both mutated to alanine. The substitution of S313 or S314 to alanine both led to drastically decreased protein expression and surface expression levels, indicating a strong effect on stability and folding of the respective MCT8 mutants. Nevertheless, in both cases uptake and efflux activities were detectable. The exchange of Ser313 to alanine resulted in a reduced $T_3$-uptake. $T_3$-efflux is likewise reduced. This indicates that a polar property is favourable for TH transport at this position. Mutation of Ser314 to alanine resulted in an even lower $T_3$ uptake activity and $T_3$-efflux consistent with low surface translocation of S314A.

## Thr503 is located within a hinge region of THM10

In the new MCT8 models, Thr503 is located at the helix discontinuity between TMH10a and TMH10b and may thus influence conformational flexibility and transport activity. The model suggests that the side chain hydroxyl may cap the helix main chain carbonyl from Gly499 (Fig. 6a). In order to probe the importance of the Cβ-hydroxyl for intramolecular interaction stabilising the unwound segment in TMH10, we mutated Thr503 to Val replacing the hydroxyl with a non-polar methyl group (Fig. 6). Expression of T503V was reduced in stably transfected MDCK1 cells. $T_3$-uptake was diminished, possibly as a result of reduced expression. Similarly, expression of T503V cRNA in *Xenopus* oocytes led to

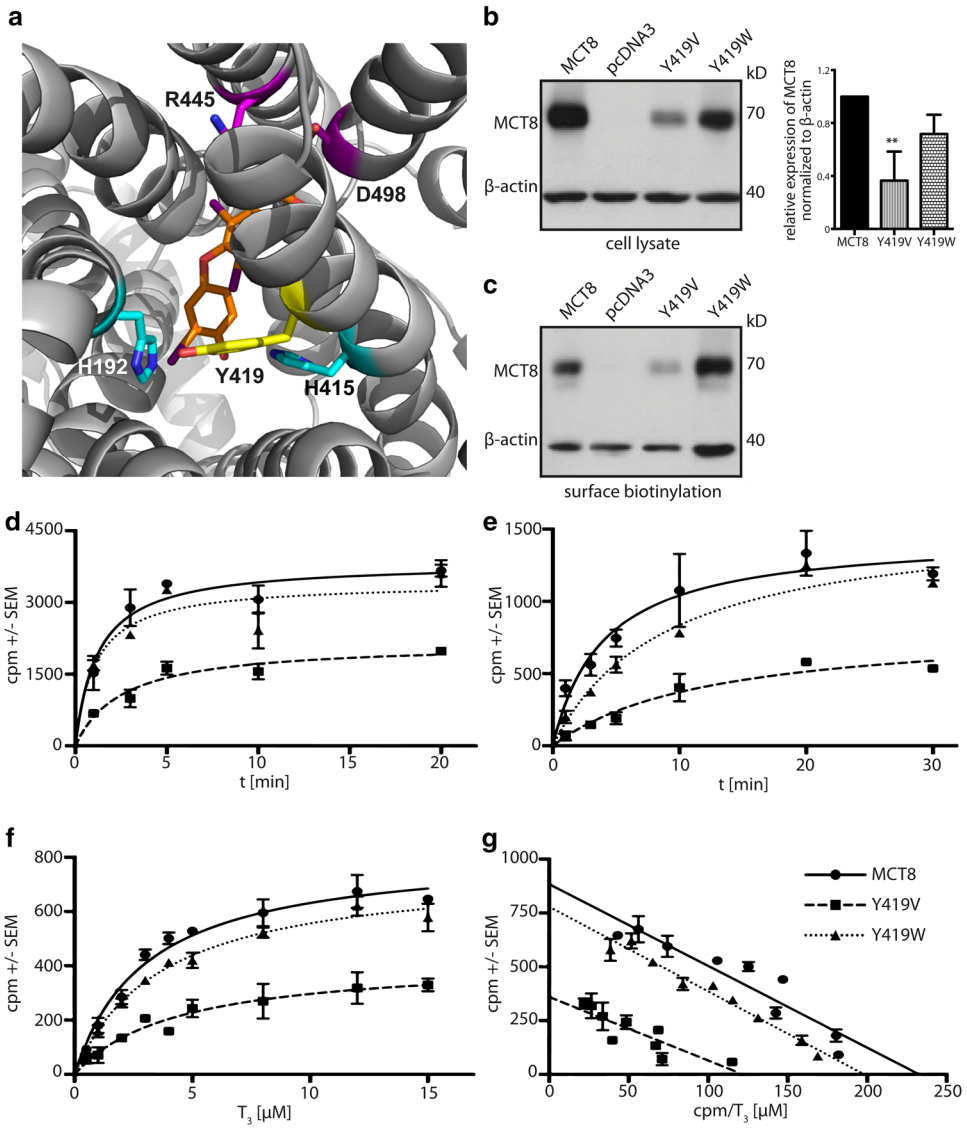


**Fig. 4** Tyr419 might close the traversing cavity in the intracellular opened state, but does not interact with the substrate. **a** Partial view of MCT8 model. Tyr419 (*sticks, yellow*) is positioned one turn above His415 (*sticks, cyan*) towards the extracellular side of MCT8 (*cartoon, grey*) and could contribute to close the traversing cavity formed by Arg445, Asp498 (*sticks, magenta*) His192 and His415 (*sticks, cyan*) in the intracellular opened state. The substrate $T_3$ is shown in *orange* as *sticks*. **b** Expression levels of different Tyr419 mutants compared to wild-type MCT8. Western blot of 25 µg whole cell homogenates against MCT8. MDCK1 cells transfected with pcDNA3 empty vector served as negative control. β-Actin was used as a loading control. Quantification of western blots was performed on four replicates by densitometry. One-way ANOVA, Dunnett's test with $^{**}p < 0.01$. **c** Surface expression of Tyr419 mutants compared to wild-type MCT8. **d** Time course uptake with 10 nM $^{125}$I-$T_3$ of MCT8$^{WT}$, Y419V and Y419W. The background of empty-vector transfected cells (pcDNA3) was subtracted from saturation curves. **e** Efflux of radioactive labelled $T_3$ by different Tyr419 mutants was measured in the media over time after loading the cells with 10 nM $^{125}$I-$T_3$ for 45 min. **f** Determination of $K_M$ values for Y419V and Y419W compared to MCT8$^{WT}$ in stably transfected MDCK1 cells. $T_3$ concentration ranges from 0.5 to 15 µM. The uptake of different concentrations of $T_3$ was measured for 3 min. Empty-vector transfected cells served as background control and values were subtracted from saturation curves. **g** Eadie–Hofstee plot of **e** with $K_M$ (MCT8) = 3.1 ± 0.4 µM; $K_M$ (Y419V) = 4.3 ± 1.0 µM; $K_M$ (Y419W) = 3.7 ± 0.4 µM

reduced $^{125}T_3$-uptake. However, the Michaelis constant was not significantly changed (MCT8$^{WT}$ = 3.0 ± 0.5 µM; T503V = 2.6 ± 0.6 µM) suggesting that $v_{max}$ is reduced which perhaps reflects impaired conformational changes. Interestingly, efflux of $T_3$ is apparently less affected than uptake. Taken together, we interpret our data as support for a role of Thr503 in conformational change (affecting the speed or accuracy of mobility) by potential

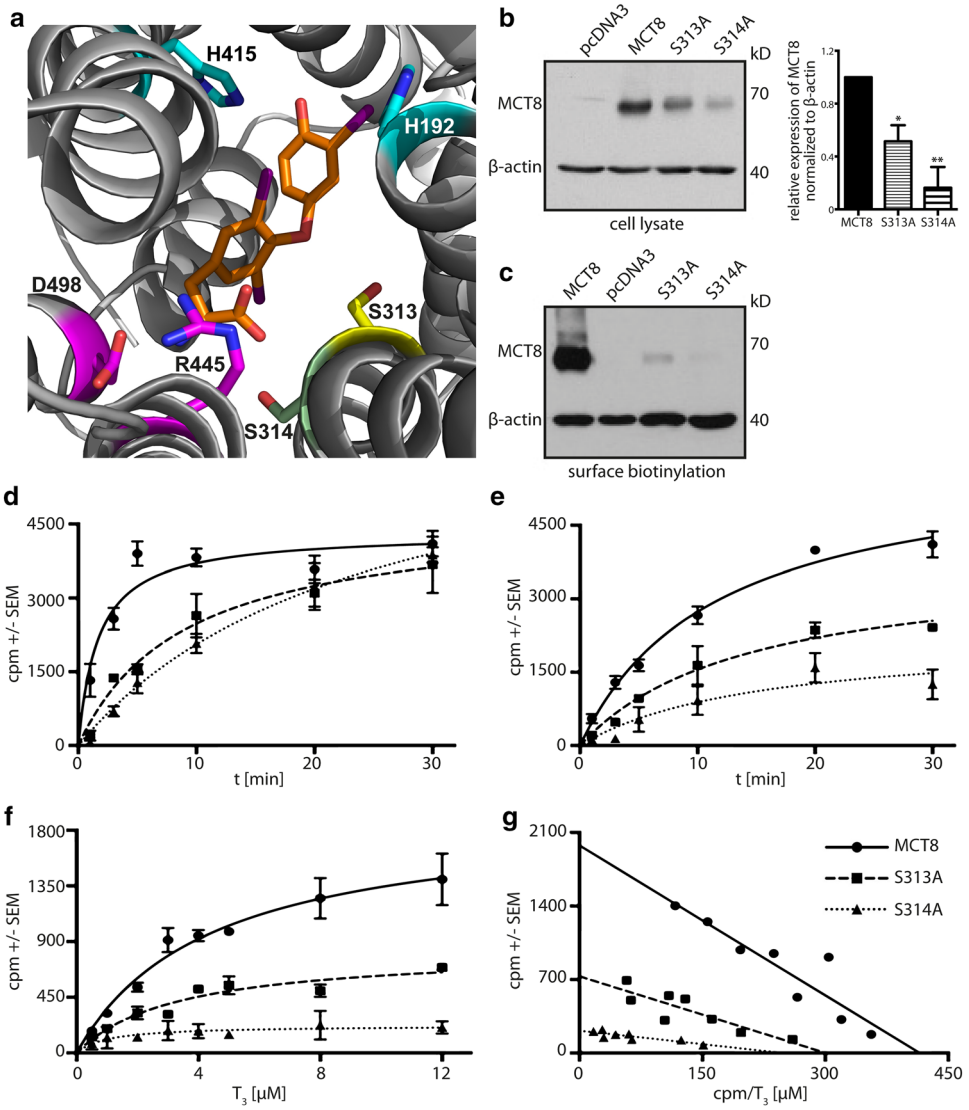


**Fig. 5** S313 and S314 provide a hydrophilic environment for the ether oxygen and the amino acid moiety of $T_3$. **a** Intermediate state between intracellular and extracellular opened conformation of the MCT8 Model (*cartoon, grey*). As previously described, binding relevant amino acids are shown as *sticks* and highlighted in *cyan* and *magenta*. The residues Ser313 (*sticks, yellow*) and Ser314 (*sticks, green*) line the central substrate channel. Ser313 is in close proximity to the ether oxygen of $T_3$. **b** Expression levels of S313A and S314A mutants compared to wild-type MCT8. Western blot of 25 µg whole cell homogenates against MCT8. MDCK1 cells transfected with pcDNA3 empty vector served as negative control. β-Actin was used as a loading control. Quantification of western blots was performed on three replicates by densitometry. One-way ANOVA, Dunnett's test with $*p<0.05$ and $**p<0.01$. **c** Cell-surface biotinylation of S313A and S314A compared to $MCT8^{WT}$. **d** Time course uptake with 10 nM $^{125}$I-$T_3$ of $MCT8^{WT}$, S313A and S314A. The background of empty-vector transfected cells (pcDNA3) was subtracted from saturation curves. **e** Efflux of radioactive labelled $T_3$ by S313A and S314A was measured in the media over time after loading the cells with 10 nM $^{125}$I-$T_3$ for 45 min. **f** Determination of $K_M$ values for S313A and S314A compared to $MCT8^{WT}$ in stably transfected MDCK1 cells. $T_3$ concentration ranges from 0.5 to 12 µM. The uptake of different concentrations of $T_3$ was measured for 3 min. Empty-vector transfected cells served as background control and values were subtracted from saturation *curves*. **g** Eadie–Hofstee plot of **e**. $K_M$ (MCT8) = 4.4 ± 0.8 µM; $K_M$ (S313A) = 3.3 ± 0.8 µM; $K_M$ (S314A) = 1.0 ± 0.6 µM

interaction with Gly499 at the helix break. The differential sensitivity of uptake and efflux towards the mutation may be compatible with our hypothesis. A direct interaction of Thr503 with substrate appears less likely given the unaltered $K_M$ value of the mutant.

## Substitution of two glutamic acids to aspartate and asparagine show no effect on T3 transport for Glu422, but enhanced uptake and efflux for Glu423

According to the MCT8 model, Glu422 is pointing into the channel leading towards the traversing cavity

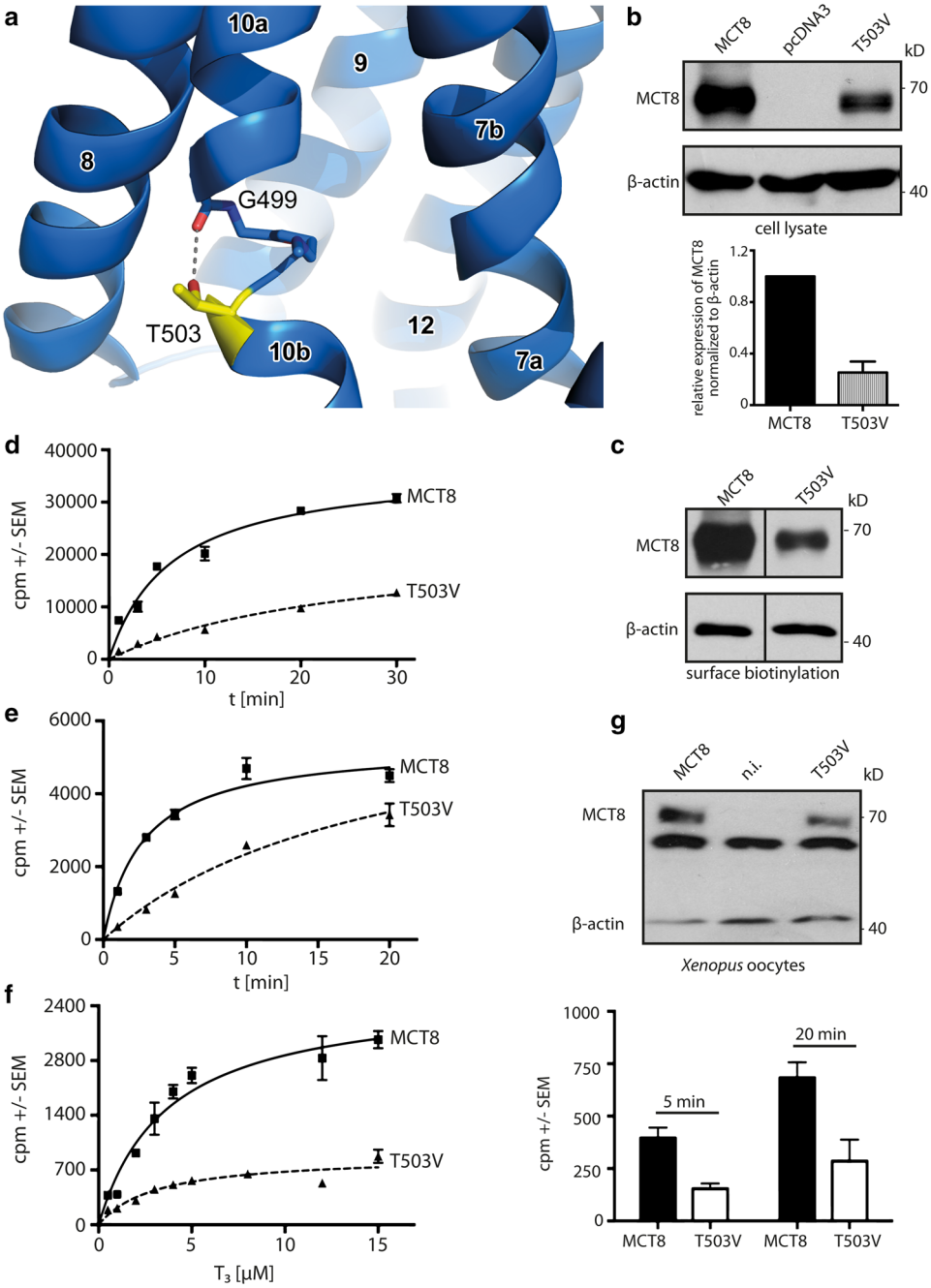


**Fig. 6** Replacing Thr503 with Val destabilises MCT8. **a** Thr503 (shown as *stick, yellow*) forms an H-bond (*dashed line*) with the carboxy-group of Gly499 (*sticks, blue*) in the model of MCT8 (*cartoon*). **b** *Upper panel* expression levels of T503V compared to wild-type MCT8 and pcDNA3 empty-vector transfected cells. Western blot of 50 µg whole cell homogenates against MCT8. β-actin served as loading control. Quantification of western blots was performed on three replicates by densitometry. *t* test, unpaired with $^{**}p < 0.01$. **c** Surface biotinylation of T503V compared to wild–type MCT8. **d** Time course experiment of 10 nM $^{125}$I-$T_3$. Empty-vector transfected cells served as background control. **e** Efflux of radioactive labelled $T_3$ by T503V stably expressing MDCK1 cells was measured in the media over time after loading the cells with 10 nM $^{125}$I-$T_3$ for 45 min. **f** Determination of $K_M$ values of T503V and MCT8$^{WT}$ of stably transfected MDCK1 cells. Empty-vector transfected cells served as background controls and were subtracted from saturation curves. $T_3$ concentration ranges from 0.5 to 15 µM. The uptake was performed for 3 min. $K_M$ (MCT8) = 3.7 ± 0.5 µM; $K_M$ (T503V) = 3.0 ± 0.7 µM. **g** Injection of *Xenopus* oocytes with 30 ng capped cRNA confirmed a lower expression of T503V compared to MCT8$^{WT}$. *Upper panel* western blot against MCT8 and β-actin (loading control). Non-injected oocytes served as negative control. *Lower panel* end point assay with 10 nM $^{125}$I-$T_3$. Non-injected cells served as background control

(Fig. 7a). Thus in the extracellular opened conformation it could be involved in guiding $T_3$ into the recognition site. Furthermore, it is located in proximity to R445 and thus might contribute to the coordination of Arg445 during the transport process. In order to investigate if charge and length of the side chain at this position are important for transport, we generated substitutions of Glu422 to asparagine and aspartate (Fig. 7). Exchange of the charged Glu422 to polar asparagine did not alter $T_3$ transport. However, shortening of the side chain, while keeping the negative charge, by substitution of Glu422 to aspartate resulted in a reduced uptake and altered efflux behaviour. This finding suggests that Glu422 is indeed

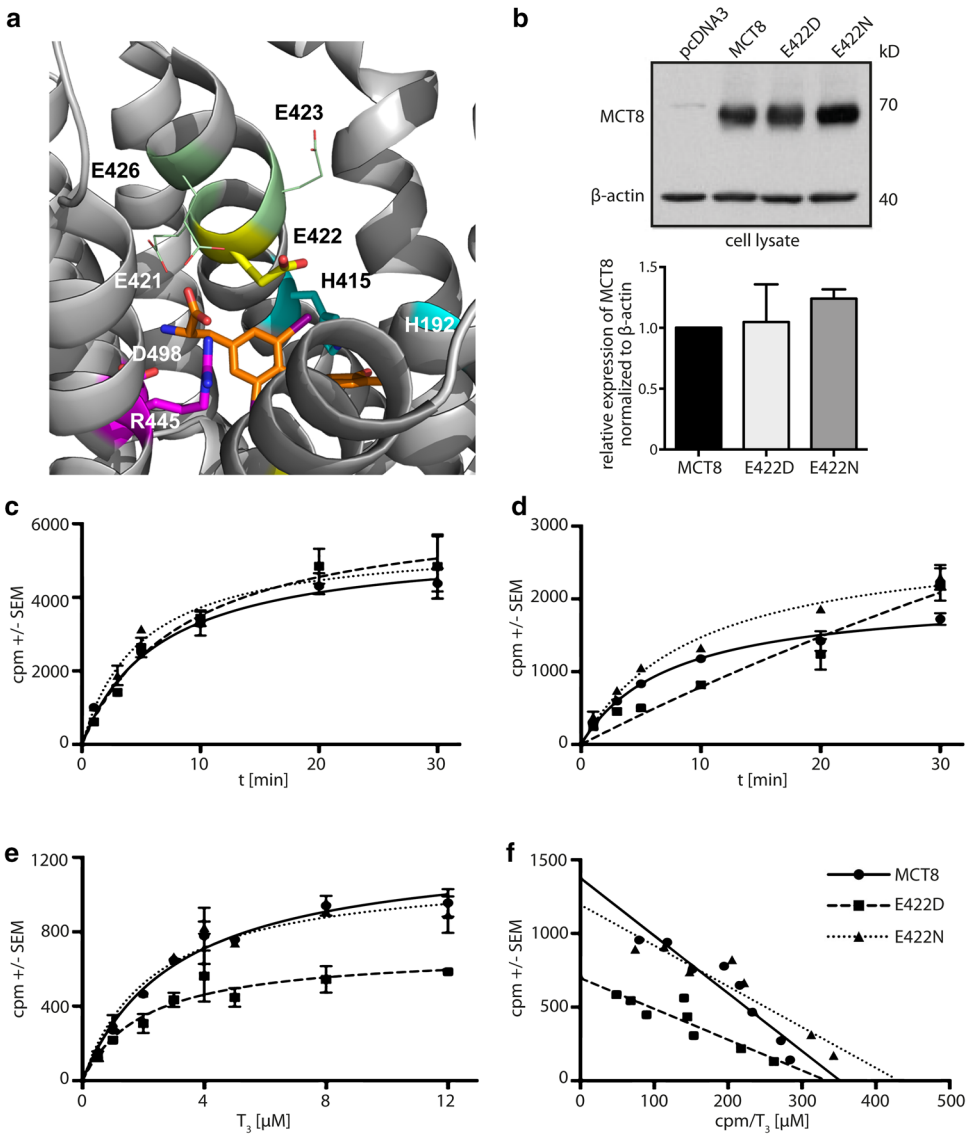


**Fig. 7** Glu422 could be involved in coordinating Arg445 and the amino acid moiety of $T_3$. **a** Extracellular opened conformation of the MCT8 Model (*cartoon, grey*). Glu422 (*sticks, yellow*) is facing to the channel leading to the binding cavity and is flanked by a stretch of negative charged residues (*lines, green*). **b** Expression levels of E422D and E422N mutants compared to wild-type MCT8. Western blot of 25 µg whole cell homogenates against MCT8. MDCK1 cells transfected with pcDNA3 empty vector served as negative control. β-Actin was used as a loading control. Quantification of western blots was performed on three replicates by densitometry. One-way ANOVA, Dunnett's test. **c** Time course uptake with 10 nM $^{125}$I-$T_3$ of MCT8$^{WT}$, E422D and E422N. The background of empty-vector transfected cells (pcDNA3) was subtracted from saturation curves. **d** Efflux of radioactive labelled $T_3$ by E422D and E422N was measured in the media over time after loading the cells with 10 nM $^{125}$I-$T_3$ for 60 min. **e** Determination of $K_M$ values for E422D and E422N compared to MCT8$^{WT}$ in stably transfected MDCK1 cells. $T_3$ concentration ranges from 0.5 to 12 µM. The uptake of different concentrations of $T_3$ was measured for 3 min. Empty-vector transfected cells served as background control and values were subtracted from saturation curves. **f** Eadie–Hofstee plot of **e**. $K_M$ (MCT8) = 3.1 ± 0.5 µM; $K_M$ (E422D) = 2.0 ± 0.5 µM; $K_M$ (E422N) = 2.4 ± 0.4 µM

involved in coordination and geometry of the $T_3$ recognition site.

In the MCT8 model, Glu423 is located extrafacial to the traversing cavity; thus it could be involved in guiding $T_3$ into the recognition site in the extracellular opened conformation (Fig. 8a). In order to investigate if the charge and length of the side chain at this position are important for transport we generated substitutions of Glu423 to asparagine and aspartate (Fig. 8). Removal of the charge and shortening of the side chain of Glu423 by substitution to

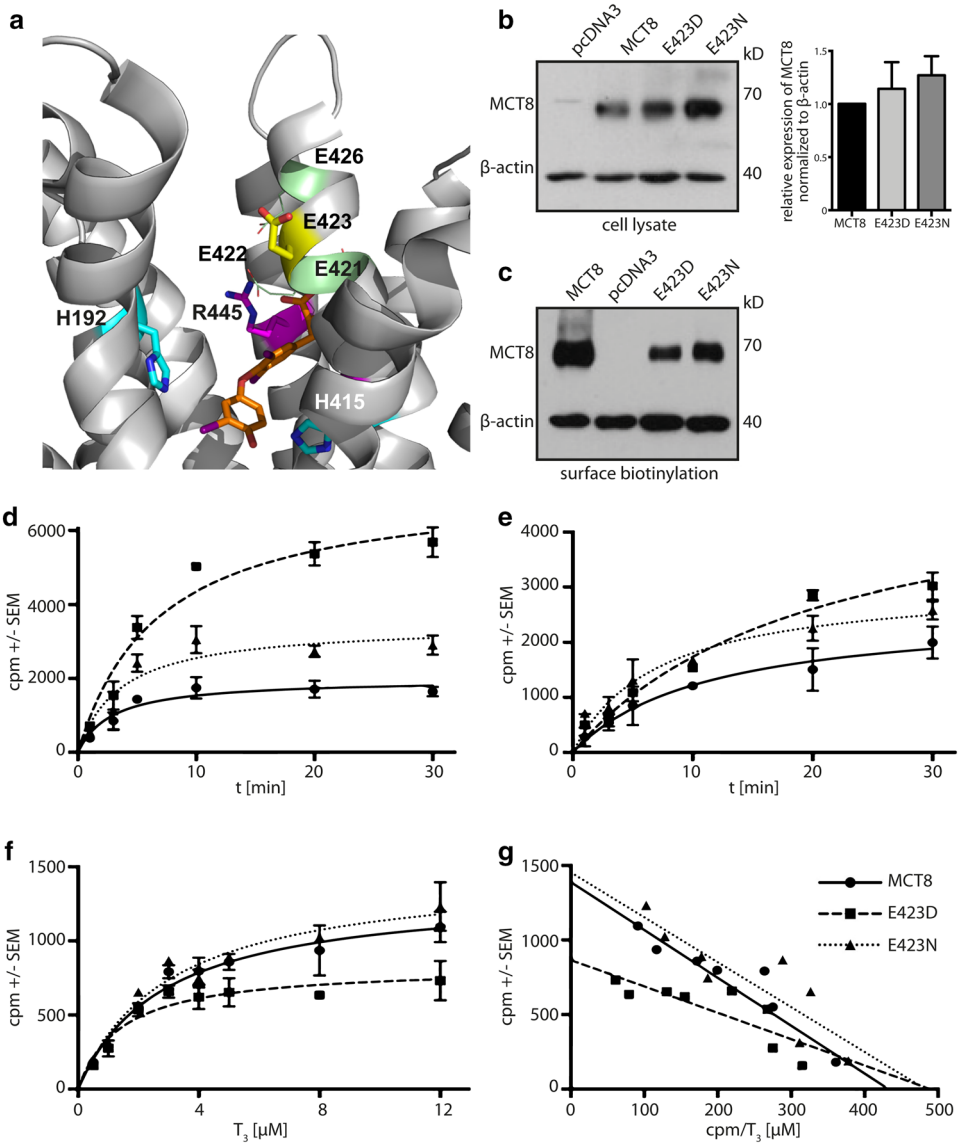


**Fig. 8** Glu423 might be involved in guiding $T_3$ to the central traversing cavity. **a** Extracellular opened conformation of the MCT8 Model (*cartoon, grey*). Glu423 (*sticks, yellow*) is facing to the channel leading to the binding cavity and is flanked by a stretch of negative charged residues (*lines, green*). **b** Expression levels of E423D and E423N mutants compared to wild-type MCT8. Western blot of 25 µg whole cell homogenates against MCT8. MDCK1 cells transfected with pcDNA3 empty vector served as negative control. β-Actin was used as a loading control. Quantification of western blots was performed on four replicates by densitometry. One-way ANOVA, Dunnett's test. **c** Surface expression of Glu423 mutants compared to wild-type MCT8. **d** Time course uptake with 10 nM $^{125}$I-$T_3$ of MCT8$^{WT}$, E423D and E423N. The background of empty-vector transfected cells (pcDNA3) was subtracted from saturation curves. **e** Efflux of radioactive labelled $T_3$ by E423D and E423N was measured in the media over time after loading the cells with 10 nM $^{125}$I-$T_3$ for 60 min. **f** Determination of $K_M$ values for E423D and E423N compared to MCT8$^{WT}$ in stably transfected MDCK1 cells. $T_3$ concentration ranges from 0.5 to 12 µM. The uptake of different concentrations of $T_3$ was measured for 3 min. Empty-vector transfected cells served as background control and values were subtracted from saturation curves. **g** Eadie–Hofstee plot of **e**. $K_M$ (MCT8) = 2.8 ± 0.4 µM; $K_M$ (E423D) = 1.4 ± 0.8 µM; $K_M$ (E423N) = 3.0 ± 0.4 µM

asparagine led to a slight enhancement of uptake and efflux compared to wild-type MCT8. Interestingly, shortening the side chain while keeping the negative charge by substitution of Glu423 to aspartate increased the uptake even more. However, efflux was not strongly altered. This indicates that Glu423 could be involved in guiding $T_3$ to the recognition side by interaction with the amine of the amino acid moiety. Side chain shortening at position 423 results in an enlargement of the entrance vestibule towards the recognition side from the extracellular side, which explains the generally enhanced uptake of both substitutions to asparagine and aspartate. A negative charge is strongly beneficial at this position, as indicated by the Michaelis constant of E423D mutant ($K_M = 1.4 \pm 0.8$ µM) compared to the one of the E423N mutant ($K_M = 3.0 \pm 0.4$ µM) and $MCT8^{WT}$ ($2.8 \pm 0.4$ µM; Fig. 8f, g).

### Is the linker region participating in transport?

Arg388 is located in the intracellular helix which is part of the linker loop connecting TMH6 and 7 between the N- and C-terminal 6 TMH-bundles. The R388Q mutation in MCT8 was initially found in an exome-sequencing effort to identify a potential gene defect in a boy with a movement disorder [38]. In our model, the Arg388 side chain points towards the intracellular vestibule leading to the substrate binding site (Fig. 9a). We initially hypothesised that the positively charged side chain of Arg388 may help attract the substrate towards the gate of the vestibule and a glutamine mutation would change the local electric field. We generated the R388Q mutant and expressed it in stably transfected MDCK1 cells and *Xenopus* oocytes along with several more Arg388 mutants. While R388Q expressed at normal levels, $T_3$-uptake was slightly reduced. This was also true for a R388M mutant. The $K_M$ of R388Q and R388M were not different from wild-type MCT8. Replacement of Arg388 by lysine appeared to reduce uptake and increase $K_M$, while protein expression remained normal. When we replaced Arg388 with glutamate, we had difficulty recovering a stably expressing MDCK1 cell line. However, when R388E was injected into *Xenopus* oocytes along with wild-type MCT8 and R388Q, transport activity was not different from the uncharged R388Q, suggesting that Arg388 is likely not critical for substrate transport or protein stability.

## Discussion

We here identified a membrane-traversing mechanism for THs by MCT8 as the two banana-shaped 6-TM-helix bundles are tilting around a central TH-interacting cavity with alternating extra- and intracellular accessibility. Moreover, we pinpoint experimentally further transport-sensitive residues that help to get a deeper insight into the molecular mechanisms of TH import and export by MCT8.

Based on a series of recently published crystal structures of sugar porters XylE, FucP and GLUT3, we have generated homology models of MCT8 in three different conformations: extracellular opened, extracellular occluded and intracellular opened. The models extend our previous inward open model based on GlpT [20] and for the first time allowed investigation of both the inward and also the outward open conformation to rationalise substrate transport through the membrane. With this information we could further identify single amino acids important for $T_3$ transport. $T_3$-docking studies from the extra- and intracellular sides revealed one central cavity for bidirectional substrate binding and traversing. Amongst others the cavity is formed by previously identified amino acids, e.g. His192, His415, Arg445 and Asp498 [20, 21, 24, 26], which can be exposed to both faces of the protein. In addition to the tilting of the N- and C-terminal domains around a central cavity, the new homology models reveal two discontinuous transmembrane helices (TMH7 and TMH10) with unwound segments residing in the middle of both. The two parts of one TMH interrupted by an unwound segment are named TMHa and TMHb (Fig. 10). Discontinuous TMHs are also found in other transporters such as sugar transporters [28, 31, 39] and even in transporter classes comprising a different fold such as LeuT, which are also accompanied by inverted repeats [18, 40]. A detailed structure–function consideration of those transmembrane helices and transport-sensitive residues that enclose the traversing cavity led to the following arrangements and conclusion (Fig. 10).

The three different MCT8 conformations indicate a particular conformational shift of the two helical segments a + b from discontinuous TMH7 and 10 relative to each other (Fig. 10a–c, right panels). This notion is of importance since many transport-sensitive residues are located in TMH7 and 10. Interestingly, several pathogenic mutations (L492P [10, 41], G495A [42], D498N [21], delF501 [43] and L512P [11]) occur on TMH10. Both TMHs are positioned parallel to each other in direct spatial proximity. His415 is located on TMH7a and the newly identified transport-sensitive residue Lys418 is located at the beginning of TMH7b. Both residues are pointing into the traversing channel of MCT8. While $T_3$ passes through the central cavity, Lys418 can alternately interact with the functional groups of the amino acid moiety of the substrate. This is the reason why a drastic mutation of positively charged Lys418 to negatively charged glutamate still enables the passage of $T_3$, while the mutation to alanine abrogates transport. Tyr419 is another amino acid located on TMH7b. Our results indicate that the aromatic residue is involved in a latch-like stabilisation of the intracellular opened state

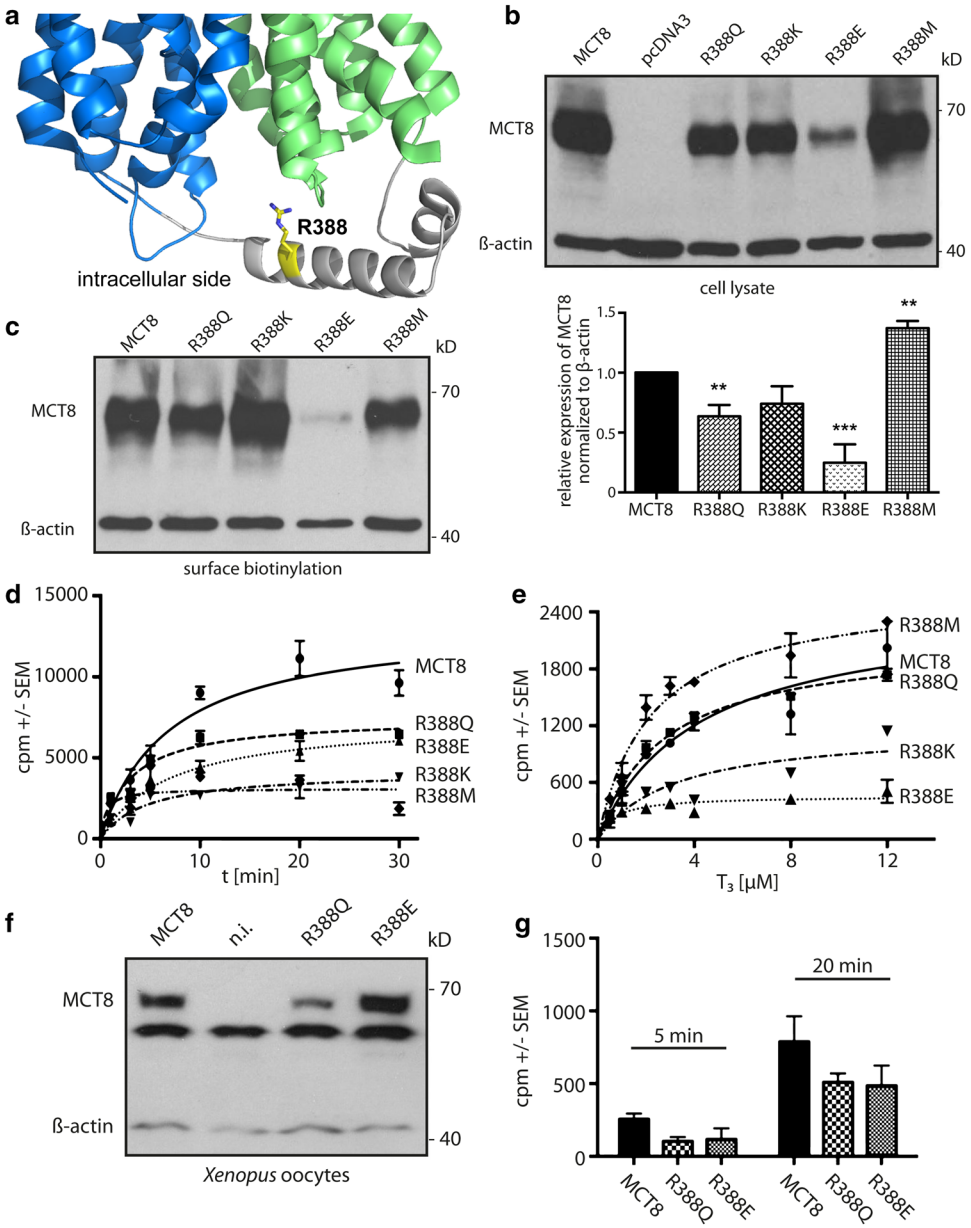


**Fig. 9** The properties of the side chain at position 388 are important for membrane localisation. **a** Arg388 (*sticks, yellow*) is located in the intracellular domain (*grey*) pointing to the vestibule of MCT8 (*cartoon*; N-terminal domain, *green*; C-terminal domain, *blue*) **b** Expression of different Arg388 mutants compared to wild-type MCT8 as positive control and empty-vector (pcDNA3) transfected cells as negative control. Western blot of 50 µg whole cell homogenates against MCT8. β-Actin served as a loading control. Quantification of western blots was performed on three replicates by densitometry. One-way ANOVA, Dunnett's test with $^{**}p<0.01$ and $^{***}p<0.001$. **c** Cell-surface expression of Arg 388 mutants compared to $MCT8^{WT}$. **d** Time course uptake of 10 nM $^{125}$I-$T_3$ in stably transfected MDCK1 cells. pcDNA3-MDCK1 served as background control. **e** Measurement of $K_M$ values of different Arg388 mutants compared to wild-type MCT8 in stably transfected MDCK1 cells. Empty-vector transfected cells served as background controls and were subtracted from saturation curves. $T_3$ concentration ranges from 0.5 to 12 µM. The uptake was performed for 3 min. $K_M$ (MCT8) = 5.5 ± 1.2 µM; $K_M$ (R388Q) = 3.9 ± 0.4 µM; $K_M$ (R388E) = 4.1 ± 0.7 µM, $K_M$ (R388K) = 6.4 ± 1.9 µM; $K_M$ (R388M) = 3.9 ± 0.7 µM. **f** Injection of *Xenopus laevis* oocytes with 30 ng capped cRNA of wild-type MCT8, R388Q and R388E. Western blot against MCT8 and β-actin (loading control). Non-injected oocytes served as negative controls. **g** End point assay in *Xenopus laevis* oocytes with 10 nM $^{125}$I-$T_3$. Non-injected oocytes served as background controls

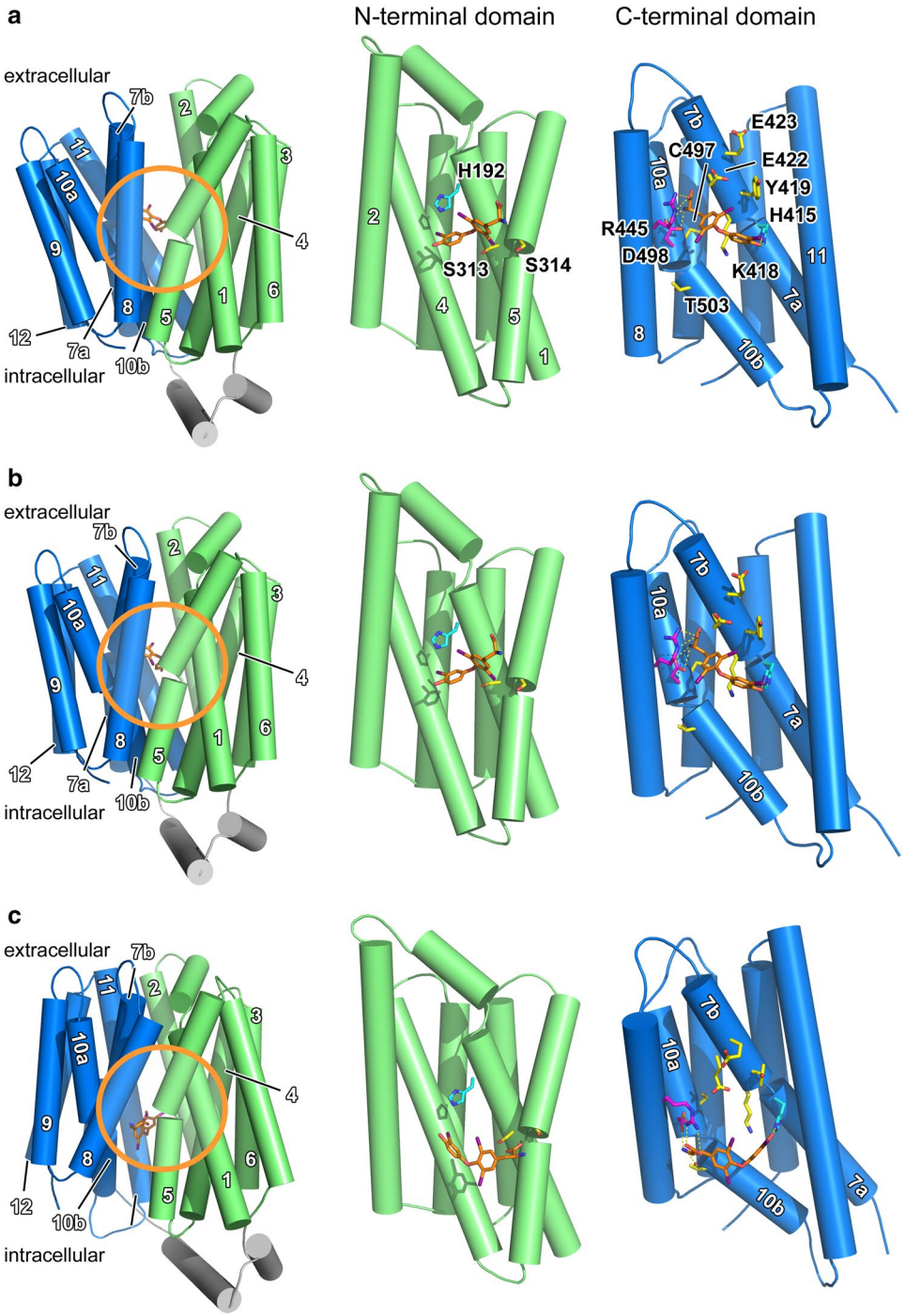


**Fig. 10** Simplified depiction of the MCT8 models in **a** the fully extracellular opened, **b** extracellular partly occluded and **c** intracellular opened conformation in side view with the two 6 TMH-bundles of the N- (*green*) and the C-terminal (*blue*) domain. The large intracellular linker is formed by helices (ICH, *grey*). Detailed positions of the lifted $T_3$ (*orange*) within the central traversing cavity (*orange circle*) with respect to the N- and C-terminal domain are shown as $T_3$ facing side view separately for the N- and C-terminal domain (*middle* and *right panels*). Most $T_3$ binding and transport-relevant residues are located on the C-terminal domain, where a slight move of the TMH10ab and 7ab (*minor*) especially at the helix-discontinuity can be observed between the extracellular (**a** *right panel*) and intracellular (**c** *right panel*) open state

by interaction with Met225 (TMH2). This intramolecular stabilisation is also supported by the recently published finding of Fischer et al. that TMH2 is involved in an dimer interface [44]. Their hypothesis that the pathogenic mutation A224T [45] could disturb this dimer interface by forming an additional H-bond with the hydroxyl group of Tyr419 [44] is consistent with our models.

Furthermore, a patch of negatively charged residues Glu421, Glu422, Glu423 and Glu426 are located on TMH7b. These residues most likely guide $T_3$ to the central traversing cavity from the extracellular side by coordinating the amine group of the amino acid moiety. Shortening of the side chain by mutating Glu423 to aspartate enlarges the space at the extracellular entrance and may explain the enhanced uptake and the unaltered efflux. However, loss of the charge by introducing an asparagine at position 423 significantly increased the Michaelis constant compared to E423D suggesting a beneficial role of the negative charge

for $T_3$ transport. This cluster of negative charged residues (Glu421, Glu422, Glu423 and Glu426) could be involved in coordination of the amine moiety of $T_3$ and the transport relevant residue Arg445 in MCT8 (Figs. 7, 8; green lines). Interestingly, this negative patch is not present in the homologue MCT10 and might be of interest for further research.

The transport-sensitive residues Cys497 and Asp498 are located at the C-terminal end of TMH10a. Both are pointing towards the traversing cavity and are thus able to interact with the substrate. This is in agreement with previously reported mutations at these positions and pCMBS accessibility of Cys497 influencing $T_3$-uptake [20, 21, 27]. The second transport-sensitive cysteine Cys481 [27] is located at the extracellular loop N-terminal to TMH10. A pCMBS derivatisation at this position can thus influence either the orientation of TMH10 or block the mobility of TMH10 probably needed for transport. The newly identified Thr503 is located at the onset of TMH10b. Thr503 probably stabilises the unwound segment of TMH10 by bending TMH10b to the interior centre of the protein (Figs. 6a, 10). This might explain why a loss of the H-bond stabilisation by the T503V mutation leads to decreased expression hinting a lower stability of the mutant. Furthermore, the loss of this H-bond could also explain why efflux of $T_3$ is less affected than uptake, since TMH10b can move further away from the interior and especially enlarge the intracellular entrance (Fig. 10c). The existence of such an unwound segment in TMH10 of MCT8 is also supported by the pathogenic deletion mutation MCT8-delPhe501, whose disturbed expression and function can be rescued by small molecule chaperones, whilst for the mutation L471P only expression but not function can be rescued [35]. Our new MCT8 models are useful to explain the differences. Phe501 is located exactly in the unwound segment between TMH10a and b close to Thr503 (Fig. 6a). Deletion of Phe501 causes a shift of Thr503 by one position in TMH10, which obviously slightly disturbs the stabilisation of the unwound segment that can be rescued by small chaperones (even by DMSO). In contrast, the lost function of the proline mutation L471P cannot be rescued by small chaperones. Leu471 is positioned in the middle of the continuous TMH9, which is not part of the traversing cavity. Thus, the proline mutation probably causes a severe fold defect in the C-terminal domain. Compendiously, we could show tilting of the two 6 TMH-bundles against each other and the rearrangements of the discontinuous TMH10 and partly of TMH7 in MCT8 which has been already reported for GLUT3 [31].

Arg445 is located in TMH8 which lies directly next to TMH10. Kinne et al. [20] suggested a possible interaction of Arg445 with Asp498 (TMH10) which was later supported by Groeneweg et al. [21]. The weak rescue of TH transport by the charge exchanging double mutant R445D/D498R compared to the respective single mutants emphasises the importance of charges at specific positions within TMHs [21]. An interaction between Arg445 and Asp498 with each other and the amino acid moiety of THs could also explain the pathogenic effect of the single mutants R445C [46], R445S [47] and D498N [48]. The loss of the charge at any of these positions disturbs the geometry and interaction pattern needed for TH transport by MCT8. In addition, Arg445 interacts with $T_3$ as a prominent partner of a His–Arg motif for clamping $T_3$ (such as His415 in TMH7). The second histidine His192 covering the central traversing cavity is located at TMH1. Until now His192 and Arg301 were the only residues interacting with the substrate identified at the N-Terminal 6 TMH-bundle. The two His–Arg clamps within the central traversing cavity (His192–Arg445 and His415–Arg445) show a comparable distance and geometry to the $T_3$ binding motif "His435–Arg282 clamp" in the TRβ: $T_3$ complex structure (PDB ID: 3gws [23]). A similar binding mode might also be feasible for His192–Arg301 and His415–Arg301. However, Arg301 is only accessible to $T_3$ in the intracellular opened conformation of MCT8. Thus, Arg301 and the corresponding potential His–Arg clamps (His192–Arg301 and His415–Arg301) seem to rather be involved in guiding the substrate in and out of the traversing cavity from the intracellular side.

The newly characterised residues Ser313 and Ser314 are located at a bulge in TMH5 in close proximity to Arg445 on TMH8. The strong effect on folding and protein stability of both S313A and S314A mutants are in full agreement with the localisation within an irregular helix compartment in our MCT8 model. Furthermore, these two serines provide a hydrophilic environment which might allow the passage of the ether oxygen atom of $T_3$ (Ser313) as well as the carboxyl group of the amino acid moiety (Ser314). In addition, they could be involved in the coordination of the amino acid group from the intracellular side as their substitution to alanine in both cases has a stronger impact on efflux than on uptake of $T_3$.

The potentially pathogenic mutant R388Q [38] which is located in the large linker loop between TMH6 and TMH7 suggests that the function of MCT8's intracellular domain might be similar to the speculated function of the intracellular helical domain of GLUT3 [31]. However, while a subtle role of Arg388 in $T_3$-transport cannot be refuted on the basis of the data presented here, our results argue against the idea that R388Q is a transport-inactive mutant. However, Arg388 might be involved in so far unknown intracellular protein–protein interactions which could contribute to the reported potential pathogenicity of R388Q.

Taken together, we here identified a membrane-traversing mechanism for THs by MCT8 as the N-terminal domain undergoes a rigid body rotation around a central TH-interacting cavity with respect to the C-terminal domain. This

allows alternating extra- and intracellular accessibility of the TH recognition-sensitive residues His192, His415, Arg445 and Asp498. After extracellular recognition by a His–Arg clamp motif $T_3$ adheres alternately to these residues and is thus conveyed through the central traversing channel and released towards the intracellular side and vice versa.

**Acknowledgements** The authors thank Simone Arndt and Tobias Lindenberg for excellent technical assistance, Catherine L. Worth for critically reading the paper before submission and acknowledge funding by Deutsche Forschungsgemeinschaft DFG THYROID TRANS ACT KR1273/5-1 (GK), Schw914/3-1 (US) and the Sherman family (US).

## References

1. Abe T, Kakyo M, Sakagami H et al (1998) Molecular characterization and tissue distribution of a new organic anion transporter subtype (oatp3) that transports thyroid hormones and taurocholate and comparison with oatp2. J Biol Chem 273:22395–22401. doi:10.1074/jbc.273.35.22395
2. Sugiyama D, Kusuhara H, Taniguchi H et al (2003) Functional characterization of rat brain-specific organic anion transporter (Oatp14) at the blood–brain barrier: high affinity transporter for thyroxine. J Biol Chem 278:43489–43495. doi:10.1074/jbc.M306933200
3. Tohyama K, Kusuhara H, Sugiyama Y (2004) Involvement of multispecific organic anion transporter, Oatp14 (Slc21a14), in the transport of thyroxine across the blood–brain barrier. Endocrinology 145:4384–4391. doi:10.1210/en.2004-0058
4. Friesema ECH, Ganguly S, Abdalla A et al (2003) Identification of monocarboxylate transporter 8 as a specific thyroid hormone transporter. J Biol Chem 278:40128–40135. doi:10.1074/jbc.M300909200
5. Friesema ECH, Jansen J, Jachtenberg J-W et al (2008) Effective cellular uptake and efflux of thyroid hormone by human monocarboxylate transporter 10. Mol Endocrinol 22:1357–1369. doi:10.1210/me.2007-0112
6. Friesema EC, Docter R, Moerings EP et al (2001) Thyroid hormone transport by the heterodimeric human system L amino acid transporter. Endocrinology 142:4339–4348
7. Zevenbergen C, Meima ME, Lima de Souza EC et al (2015) Transport of iodothyronines by human L-type amino acid transporters. Endocrinology 156:4345–4355. doi:10.1210/en.2015-1140
8. Kinne A, Wittner M, Wirth EK et al (2015) Involvement of the L-type amino acid transporter Lat2 in the transport of 3,3′-diiodothyronine across the plasma membrane. Eur Thyroid J 4:42–50. doi:10.1159/000381542
9. Schweizer U, Johannes J, Bayer D, Braun D (2014) Structure and function of thyroid hormone plasma membrane transporters. Eur Thyroid J 3:143–153. doi:10.1159/000367858
10. Friesema ECH, Grueters PA, Biebermann H et al (2004) Association between mutations in a thyroid hormone transporter and severe X-linked psychomotor retardation. Lancet 364:1435–1437. doi:10.1016/S0140-6736(04)17226-7
11. Dumitrescu AM, Liao XH, Best TB et al (2004) A novel syndrome combining thyroid and neurological abnormalities is associated with mutations in a monocarboxylate transporter gene. Am J Hum Genet 74:168–175
12. Schwartz CE, May MM, Carpenter NJ et al (2005) Allan–Herndon–Dudley syndrome and the monocarboxylate transporter 8 (MCT8) gene. Am J Hum Genet 77:41–53
13. Dumitrescu AM, Liao XH, Weiss RE et al (2006) Tissue-specific thyroid hormone deprivation and excess in monocarboxylate transporter (Mct) 8-deficient mice. Endocrinology 147:4036–4043. doi:10.1210/en.2006-0390
14. Trajkovic M, Visser T, Mittag J (2007) Abnormal thyroid hormone metabolism in mice lacking the monocarboxylate transporter 8. J Clin Invest 117:627–635. doi:10.1172/JCI28253.A
15. Wirth EK, Roth S, Blechschmidt C et al (2009) Neuronal 3′,3,5-triiodothyronine (T3) uptake and behavioral phenotype of mice deficient in Mct8, the neuronal T3 transporter mutated in Allan–Herndon–Dudley syndrome. J Neurosci 29:9439–9449
16. Mayerl S, Müller J, Bauer R et al (2014) Transporters MCT8 and OATP1C1 maintain murine brain thyroid hormone homeostasis. J Clin Invest 124:1987–1999. doi:10.1172/JCI70324
17. Roberts LM, Woodford K, Zhou M et al (2008) Expression of the thyroid hormone transporters monocarboxylate transporter-8 (SLC16A2) and organic ion transporter-14 (SLCO1C1) at the blood–brain barrier. Endocrinology 149:6251–6261. doi:10.1210/en.2008-0378
18. Shi Y (2013) Common folds and transport mechanisms of secondary active transporters. Annu Rev Biophys 42:51–72. doi:10.1146/annurev-biophys-083012-130429
19. Huang Y, Lemieux MJ, Song J et al (2003) Structure and mechanism of the glycerol-3-phosphate transporter from Escherichia coli. Science 301(80):616–620. doi:10.1126/science.1087619
20. Kinne A, Kleinau G, Hoefig CS et al (2010) Essential molecular determinants for thyroid hormone transport and first structural implications for monocarboxylate transporter 8. J Biol Chem 285:28054–28063. doi:10.1074/jbc.M110.129577
21. Groeneweg S, Friesema ECH, Kersseboom S et al (2014) The role of Arg445 and Asp498 in the human thyroid hormone transporter MCT8. Endocrinology 155:618–626. doi:10.1210/en.2013-1521
22. Ye L, Li YL, Mellström K et al (2003) Thyroid receptor ligands. 1. Agonist ligands selective for the thyroid receptor β1. J Med Chem 46:1580–1588. doi:10.1021/jm021080f
23. Nascimento AS, Dias SMG, Nunes FM et al (2006) Structural rearrangements in the thyroid hormone receptor hinge domain and their putative role in the receptor function. J Mol Biol 360:586–598. doi:10.1016/j.jmb.2006.05.008
24. Braun D, Lelios I, Krause G, Schweizer U (2013) Histidines in potential substrate recognition sites affect thyroid hormone transport by monocarboxylate transporter 8 (MCT8). Endocrinology 154:2553–2561. doi:10.1210/en.2012-2197
25. Kleinau G, Schweizer U, Kinne A et al (2011) Insights into molecular properties of the human monocarboxylate transporter 8 by combining functional with structural information. Thyroid Res 4 (Suppl 1):S4. doi:10.1186/1756-6614-4-S1-S4
26. Groeneweg S, Lima de Souza EC, Visser WE et al (2013) Importance of His192 in the human thyroid hormone transporter MCT8 for substrate recognition. Endocrinology 154:2525–2532. doi:10.1210/en.2012-2225
27. Lima de Souza EC, Groeneweg S, Visser WE et al (2013) Importance of cysteine residues in the thyroid hormone transporter MCT8. Endocrinology 154:1948–1955. doi:10.1210/en.2012-2101
28. Quistgaard EM, Löw C, Moberg P et al (2013) Structural basis for substrate transport in the GLUT-homology family of monosaccharide transporters. Nat Struct Mol Biol 20:766–768. doi:10.1038/nsmb.2569

29. Sun L, Zeng X, Yan C et al (2012) Crystal structure of a bacterial homologue of glucose transporters GLUT1-4. Nature 490:361–366. doi:10.1038/nature11524
30. Medlock AE, Dailey TA, Ross TA et al (2007) A pi-helix switch selective for porphyrin deprotonation and product release in human ferrochelatase. J Mol Biol 373:1006–1016. doi:10.1016/j.jmb.2007.08.040
31. Deng D, Sun P, Yan C et al (2015) Molecular basis of ligand recognition and transport by glucose transporters. Nature 526:391–396. doi:10.1038/nature14655
32. Dang S, Sun L, Huang Y et al (2010) Structure of a fucose transporter in an outward-open conformation. Nature 467:734–738. doi:10.1038/nature09406
33. Schrödinger LLC (2016) The PyMOL molecular graphics system, Version 1.8.0.1
34. Braun D, Kim TD, le Coutre P et al (2012) Tyrosine kinase inhibitors noncompetitively inhibit MCT8-mediated iodothyronine transport. J Clin Endocrinol Metab 97:E100–E105. doi:10.1210/jc.2011-1837
35. Braun D, Schweizer U (2015) Efficient activation of pathogenic ΔPhe501 mutation in monocarboxylate transporter 8 by chemical and pharmacological chaperones. Endocrinology 156:4720–4730. doi:10.1210/en.2015-1393
36. Johannes J, Braun D, Kinne A et al (2016) Few amino acid exchanges expand the substrate spectrum of monocarboxylate transporter 10. Mol Endocrinol. doi:10.1210/me.2016-1037
37. Kinne A, Roth S, Biebermann H et al (2009) Surface translocation and tri-iodothyronine uptake of mutant MCT8 proteins are cell type-dependent. J Mol Endocrinol 43:263–271. doi:10.1677/JME-09-0043
38. Fu J, Refetoff S, Dumitrescu AM, Weiss RE (2014) OR29-3: whole-exome sequencing identified a novel MCT8 gene mutation in a child with mild cognitive, motor and behavior abnormalities. Endocr Rev 35:OR29-OR33. doi:10.1210/endo-meetings.2014.THPTA.1.OR29-3
39. Nomura N, Verdon G, Kang HJ et al (2015) Structure and mechanism of the mammalian fructose transporter GLUT5. Nature 526:397–401. doi:10.1038/nature14909
40. Screpanti E, Hunte C (2007) Discontinuous membrane helices in transport proteins and their correlation with function. J Struct Biol 159:261–267. doi:10.1016/j.jsb.2007.01.011
41. Jansen J, Friesema ECH, Kester MHA et al (2008) Genotype-phenotype relationship in patients with mutations in thyroid hormone transporter MCT8. Endocrinology 149:2184–2190. doi:10.1210/en.2007-1475
42. Anik A, Kersseboom S, Demir K et al (2014) Psychomotor retardation caused by a defective thyroid hormone transporter: report of two families with different MCT8 mutations. Horm Res Paediatr 82:261–271. doi:10.1159/000365191
43. Visser WE, Jansen J, Friesema ECH et al (2009) Novel pathogenic mechanism suggested by ex vivo analysis of MCT8 (SLC16A2) mutations. Hum Mutat 30:29–38. doi:10.1002/humu.20808
44. Fischer J, Kleinau G, Müller A et al (2015) Modulation of monocarboxylate transporter 8 oligomerization by specific pathogenic mutations. J Mol Endocrinol 54:39–50. doi:10.1530/JME-14-0272
45. Raymond L, Whibley A, Price S et al (2008) Raised T3 levels and mutations in MCT8(SLC16A2) cause X-linked cerebral palsy and mental retardation. Eur J Hum Genet 16:60
46. Friesema ECH, Visser WE, Visser TJ (2010) Genetics and phenomics of thyroid hormone transport by MCT8. Mol Cell Endocrinol 322:107–113. doi:10.1016/j.mce.2010.01.016
47. Ono E, Ariga M, Oshima S et al (2016) Three novel mutations of the MCT8 (SLC16A2) gene: individual and temporal variations of endocrinological and radiological features. Clin Pediatr Endocrinol 25:23–35. doi:10.1297/cpe.25.23
48. Ugrasbul F, Ardinger HH (2009) A patient presenting with central hypothyroidism, developmental delay and poor head control. Should we be checking T3 levels? Horm Res 72(Suppl 3):458–459. doi:10.1159/000239668